Bull. Disas. Prev. Res. Inst., Kyoto Univ., Vol. 40, Part 1, No. 345, March, 1990

Numerical Calculation of Linear Wave Propagation in the Coastal Zone

By Takao YAMASHITA, Yoshito TSUCHIYA, Masafumi MATSUYAMA and Tsuyoshi SUZUKI

(Manuscript received on January 9, 1990)

Abstract

Numerical calculation method of short waves in the coastal zone is developed using the transformed mild slope equation, which is derived by transforming the elliptic MSE into the system of three first-order hyperbolic equations (H-MSE). The derived system of equations is solved by ADI method with employing the artificial boundary condition, called sponge layer to perform an effective computation.

Including additional effects of energy dissipation due to wave breaking and wave-current interaction, it is attempted to raise model's level up to the version which can calculate wave fields in the surf zone as well as around the coastal structures with an accuracy for engineering practices. After fundamental model tests, it is shown that the developed short-wave model predicts the stationary wave field in which effects of refraction, diffraction, reflection and energy dessipation are simultaneously considered.

1. Introduction

Short-wave prediction is the most important and fundamental work in the field of coastal engineering. However, even if under the assumption of periodic wave, it is not always easy to calculate the wave field in the coastal area where man-made structures and wave breaking exist. Several effects, such as refraction, diffraction, reflection, dissipation, non-linearity and wave-current interaction, simultaneously come to play a significant role for the wave propagation in this region.

One of the most general approaches of shor-wave calculation so far is based on the time-dependent, vertically integrated Boussinesq equations (Abbott et al. 1981)[1], which are able to simulate unsteady two-dimensional flows in vertically homogenous fluids and short-waves with weak non-linearity because of its inclusion of non-linear and dispersion terms. The disadvantage of this approach is a small range of applicability, *i.e.* the Ursell number $U_r \simeq 1$.

Since the initial development of the mild-slope equation (MSE) by Berkhoff (1972)[2], a great strides have been made in the modelling of linear water waves under the simultaneous consideration of diffraction, refraction and reflection. The MSE supplements the more copmrehensive approach base on the Boussinesq equations. For some applications the MSE is preferable.

This model is based on the theory of simple harmonic linear water waves, and so the effects of nonlinearity and energy dissipation by bottom friction or breaking are not

taken into account. The motion of water is assumed to be irrotational and the problem is described by a two-dimensional field equation of elliptic type due to the vertical integration from the bottom to surface. Employing additional assumptions, energy dissipation and wave-current interaction, this model has been developed to the useful version for various engineering practices.

The elliptic MSE is most commonly solved by the finite element method, *e.g.* Berkhoff (1976)[3]. However, because this solution method usually requires a lot of computational effort in the case of a large area, a simplification of the equation and/or the effective numerical method have to be successfully attempted. Radder (1979)[4] derived the so-called parabolic approximation of MSE by the splitting matrix method, in which the diffraction in the direction of propagation is neglected and the diffraction along the wave front is considered. This method is applicable to computations of wave propagation under the condition that the main wave direction is maintained and reflection effect is negligible. The parabolic MSE governing foward-scattered wave motion has the advantage of reducing the computing time and capacity. Because of this advantage, a lot of efforts have done to make this model applicable for engineering purposes, *e.g.* Tsuchiya et al. (1984)[5].

Warren et al. (1985)[6] and Copeland (1985)[7] has developed an alternative elliptic stationary MSE by transforming the equation into the system of three first-order hyperbolic equations (iterative form). Copeland (1985)[7] solved the resulting system of equations using an explicit finite difference scheme and showed that this method offers the advantage of reducing computing time to get results of linear wave field (height and direction) with boundary conditions of arbitrary reflecting/transmitting power. In this paper we name this type of wave model "hyperbolic MSE (H-MSE) model". Madesen and Larsen (1987)[8] developed an approach to solve the H-SME using the ADI (Alternating Direction Implicit) finite difference scheme and a time-varying time step technique.

Ito and Tanimoto (1972)[9] showed a method to calculate the refraction-diffraction combined short wave propagation in terms of a system of linear long-wave equations which describes the amplitude variation of simple harmonic waves. Even though their basic equations are not completely equivalent to the elliptic MSE, the idea of the H-MSE method probably originates in this approach.

In engineering applications of short wave field calculation, one of big restrictions is the fact that a computational domain is virtually infinite. However, economical constrains necessitate that the domain is limited as far as possible. Larsen and Dancy (1983)[10] described that almost perfect absorption of waves can be obtained by the sponge layer. This approach is based on an artificial damping which is introduced in the governing equations by applying a friction factor in a few grid lines near the closed boundaries. The sponge layer has very broad-banded damping characteristics in the direction of wave propagation, however, it causes problem of artificial diffraction in the direction of wave crest line. Using technique of the sponge layer will be discussed in this paper.

Consideration of the effect of a nonlinear dispersion relation is also important for the wave propagation in shallow water, such as just before breaking, which has been ex-

amined and incorporated into the parabolic MSE by Kirby and Dalrymple (1986)[11]. Especially in the nearshore dynamic system, the nonlinear wave-current interaction must be considered, which might be essential in a generation of nearshore circulation.

In this paper, modifications of the elliptic MSE for engineering practices are investigated and the H-MSE in the wave-current combined system is derived in section 2. The numerical calculation algorithm of the H-MSE is discussed in section 3. Several model tests of the developed computer code are performed and demonstrated in section 4.

2. Basic equation for wave-current system

A wave-current interaction system plays an important role in the coastal hydraulics which is basis of predicting beach topography changes and nearshore circulation. For these purposes of nearshore environmental problems, the refraction-diffraction combined linear wave theory has been developed as a useful tool for the computer simulation of wave-current system in the coastal zone. In the following, the previous works on the MSE for the wave train propagating on the slowly varying depth and with currents is summarized and discussed, then the H-MSE in the wave-current system with energy dissipation effect due to wave breaking is derived.

2.1 The elliptic MSE in the wave-current system

Taking three dimensional rectangular coordinates (x, y, z), such that the x- and y-axes are horizontal and z- axis is vertically upwards (see **Fig. 1**), the time-dependent MSE with currents is derived as Eq. (1), in which the energy dissipation due to wave breaking or bottom friction is included by the term of $i\sigma W\Phi$ (*e.g.* Kirby (1984)[11]).

$$\frac{D^2\Phi}{Dt^2}+(\nabla\cdot\vec{U})\frac{D\Phi}{Dt}+\left(\frac{D}{Dt}\nabla\cdot\vec{U}\right)\Phi-\nabla\cdot(CC_g\nabla\Phi)$$

$$+(\sigma^2-K^2CC_g-i\sigma W)\Phi=0 \tag{1}$$

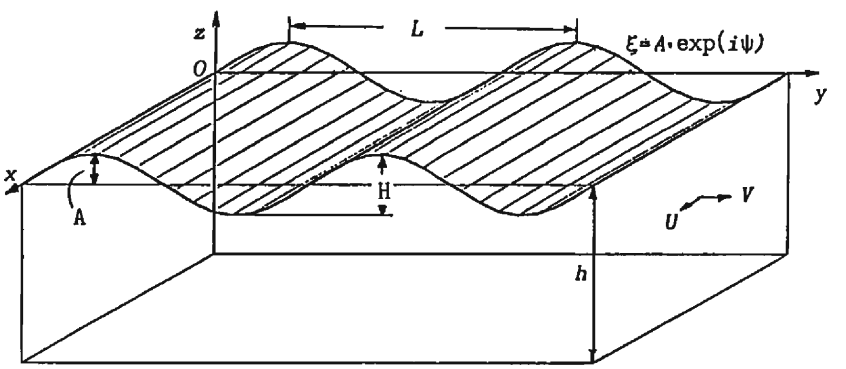

Fig. 1. Coordinate system and definition of variables.

Where the Lagrangian derivative operator D/Dt is

$$\frac{D}{Dt}=\frac{\partial}{\partial t}+U_j\frac{\partial}{\partial x_j} \tag{2}$$

and, Φ is the velocity potential of linear wave motion, $\vec{U}$: the vertically uniform current vector, C and C_g: the wave celerity and group velocity, W: the dissipation factor, ∇: a horizontal gradient operator, $\vec{k}$: wave number vector, h: water depth, g: the gravitational acceleration. In the wave-current system, two wave frequencies of the intrinsic wave frequency σ and the observed (apparent) frequency ω are defined as:

$$\omega=\sigma+\vec{k}\cdot\vec{U} \tag{3}$$

where the σ is functional dependent on $\vec{k}$ with the dispersion relation of

$$\sigma^2=gk\tanh kh \tag{4}$$

Because of the validity that the time and space scales of wave motion are small compared with currents, the local properties of the wave train can be specified by $\Phi=a\exp(i\Psi)$, where a is the local amplitude and Ψ is the phase. Assuming the phase $\Psi(\vec{k}, \omega; \vec{x}, t)$ is slowly varying function in time and space, local wave number and frequency are defined by

$$\vec{k}=\nabla\Psi \qquad \text{and} \qquad \omega=-\frac{\partial\Psi}{\partial t} \tag{5}$$

From the first equation of Eq. (5), the irrotational condition of the local wave number, $\nabla\times\vec{k}=0$, is immediately obtained. Eliminating the phase function from Eq. (5), we get

$$\frac{\partial\vec{k}}{\partial t}+\nabla\omega=0 \tag{6}$$

This equation means that $\vec{k}$ is a phase density (the number of equal phase lines per unit distance) and ω is a phase flux (the number of phase lines passing a fixed point).

Assuming the steady sate and neglecting the higher order terms such as

$$U_i\frac{\partial U_i}{\partial x_i}\frac{\partial\Phi}{\partial x_i},\quad U_i\frac{\partial U_j}{\partial x_i}\frac{\partial\Phi}{\partial x_j},\quad U_i\frac{\partial U_j}{\partial x_j}\frac{\partial\Phi}{\partial x_i},\quad U_iU_j\frac{\partial\Phi}{\partial x_i\partial x_j}\quad\text{and}\quad {U_i}^2\frac{\partial^2\Phi}{\partial x_i^2}$$

Eq. (1) is finally simplified as:

$$\nabla\cdot(CC_g\nabla\Phi)+2i\omega(\vec{U}\cdot\nabla\Phi)+i\omega\nabla\cdot\vec{U}\Phi-(\sigma^2-k^2CC_g-\omega^2-i\sigma W)\Phi=0 \tag{7a}$$

When no steady current is assumed Eq. (7a) is written as:

$$\nabla\cdot(CC_g\nabla\Phi)+(k^2CC_g+i\sigma W)\Phi=0 \tag{7b}$$

2.2 Introduction of energy dissipation effect due to wave breaking

In order to introduce the dissipation effect to the MSE we consider the energy conservation described by the wave equation. Assuming the velocity potential by the form

of $\Phi=a(\vec{x})\exp i\Psi(\vec{x})$ and substituting it into Eq. (7b), we get the propagation relation from real part and the energy conservation from imaginary part, respectively.

$$(\nabla\Psi)^2=k^2+\frac{\nabla CC_g}{CC_g}\cdot\frac{\nabla a}{a}+\frac{\nabla^2 a}{a} \tag{8a}$$

$$\nabla\cdot(CC_g a^2\nabla\Psi)+a^2\sigma W=0 \tag{8b}$$

As the wave energy is given by $E=1/2\rho gA^2$ (A: the wave amplitude, $A=\sigma a/g$), Eq. (8b) is rewritten as:

$$\nabla\cdot\left(\frac{\vec{k}}{|\vec{k}|}EC_g\right)+EW=0 \tag{9}$$

Expressing energy dissipation rate with D, the energy conservation equation is expressed by

$$\nabla\cdot(E\vec{C_g})+D=0 \tag{10}$$

Consequently the dissipation function W in the MSE is defined by the relation of the wave energy dissipation rate D to the wave energy density E as:

$$W=\frac{D}{E} \tag{11}$$

Three types of formulation may be proposed to evaluate the energy dissipation rate due to wave breaking.

(1) Type-1 (wave energy fulux model)

$$D=\lambda\frac{EC_g}{d}$$

where d: the total water depth.

(2) Type-2 (bore model)

$$D=\frac{\rho gH^3}{4hT}$$

where T: wave period.

(3) Type-3 (breaker eddy model)

$$D=\lambda_e\frac{E_e l_e}{T_e h}$$

where E_e, T_e and l_e are energy, period and length scale of the surface eddy of breaking wave.

The most commonly used model is Type-1. Here we employ the model proposed by Izumiya and Horikawa (1983)[13] which is formulated as:

$$D=\gamma_*\beta\frac{E^{3/2}}{\rho^{1/2}(h+\bar{\xi})^{3/2}}\left(\frac{2C_g}{C}-1\right)^{1/2} \tag{12}$$

where $\bar{\xi}$ is the mean water level,

$$\gamma_* \beta = \beta_0 (M_*^2 - M_{*s}^2)^{1/2} \quad \text{and} \quad M_*^2 = \frac{C_g}{C} \frac{E}{\rho g (h+\bar{\xi})^2} \tag{13}$$

They suggested the model parameters of $\beta_0 = 1.8$, $M_{*s} = 0.009$ to simulate wave reforming.

In their fomulation of energy dissipation rate due to breaking is rewritten by the ratio of breaker height to local depth H/h, as:

$$D = 0.08 (H_r^2 - H_{rc}^2)^{1/2} H_r \frac{E c_g}{h} \tag{14}$$

where $H_r = H/h$, h is the local water depth. In the actual calculation we replaced the total water depth to the local water depth from the still water level.

2.3 The hyperbolic MSE

One of economical methods to solve the elliptic partial differential equation is to transform it into system of first order partial differential equations. Applying this method to the MSE, the transformed version of MSE (H-MSE) in the wave-current system is derived.

For a simple explanation of derivation, the original MSE is firstly used and finally the H-MSE with disppation and current interaction terms is shown.

Assuming a simple harmonic solution and using the velocity potential of

$$\Phi = \frac{g\xi}{i\sigma} = \frac{gA}{i\sigma} \exp(i\Psi) \tag{15}$$

the original MSE is rewritten as:

$$\nabla \cdot (CC_g \nabla \xi) - \frac{C_g}{C} \frac{\partial^2 \xi}{\partial t^2} = 0 \tag{16}$$

As shown by Madsen and Larsen (1987)[8], the equivalent hyperbolic system to Eq. (16) is,

$$\frac{\partial P^*}{\partial x} + \frac{\partial Q^*}{\partial y} + \frac{C_g}{C} \frac{\partial \xi}{\partial t} = 0 \tag{17}$$

$$\frac{\partial P^*}{\partial t} + CC_g \frac{\partial \xi}{\partial x} = 0 \tag{18}$$

$$\frac{\partial Q^*}{\partial t} + CC_g \frac{\partial \xi}{\partial y} = 0 \tag{19}$$

where P^*, Q^* are pseudo fluxes. Time evolutional solution actually indicates iteration toward the steady solution of the elliptic MSE. As solutions can be assumed by the form of

$$\xi = S(x, y, t) \exp(-i\omega t) \tag{20}$$

$$P^*=P(x, y, t)\exp(-i\omega t) \tag{21}$$

$$Q^*=Q(x, y, t)\exp(-i\omega t) \tag{22}$$

the harmonic variation is extracted from the system of equations. P, Q and S are complex functions with respect to x, y, t, which depict slow variation of wave motion. Consequently the resultant form of the H-MSE is obtained as:

$$\frac{\partial P}{\partial x}+\frac{\partial Q}{\partial y}+\frac{C_g}{C}\frac{\partial S}{\partial t}-i\omega S=SS \tag{23}$$

$$\frac{\partial P}{\partial t}-i\omega P+CC_g\frac{\partial S}{\partial x}=0 \tag{24}$$

$$\frac{\partial Q}{\partial t}-i\omega Q+CC_g\frac{\partial S}{\partial y}=0 \tag{25}$$

using the relations of

$$\frac{\partial P^*}{\partial t}=-CC_g\frac{\partial \xi}{\partial x} \quad \text{and} \quad \frac{\partial Q^*}{\partial t}=-CC_g\frac{\partial \xi}{\partial y} \tag{26}$$

The elliptic MSE (7a) in the wave-current system with energy disspation is transformed into the equivalent system of equations which is same as that of nearly horizontal flow in the shallow water as:

$$\frac{\partial P}{\partial x}+\frac{\partial Q}{\partial y}-\frac{1}{\omega^2}\left\{\sigma^2-k^2CC_g-\omega^2-i\sigma W-i\omega\left(\frac{\partial U}{\partial x}+\frac{\partial V}{\partial y}\right)\right\}\left(\frac{\partial S}{\partial t}-i\omega S\right)$$

$$+2i\omega\left(\frac{UP}{CC_g}+\frac{VQ}{CC_g}\right)=SS \tag{27}$$

$$\frac{\partial P}{\partial t}-i\omega P+CC_g\frac{\partial S}{\partial x}=0 \tag{28}$$

$$\frac{\partial Q}{\partial t}-i\omega Q+CC_g\frac{\partial S}{\partial y}=0 \tag{29}$$

where SS is the wave generation term defined by

$$SS=\frac{\Delta S}{\Delta x\Delta y}CS_0 \tag{30}$$

where Δx and Δy are mesh-sizes in the x and y directions, C is wave celerity and Δs: the width of the wave front inside a grid, S_0: the complex surface elevation function specified on the generation grid points.

3. Numerical calculation algorithm

The derived system of partial differential equations is same type as the linear long

wave equation system. The effective finite difference algorithm for this system is ADI (Alternating Direction Implicit) scheme, which can be economically solved by the double sweep method. In this section, the outlines of the solving method employed is presented.

3.1 Difference equations of H-MSE

The H-MSE described by Eqs. (27)–(29) are discretized by means of the ADI scheme of finite difference method. Defining the complex variables S, P and Q on a space-staggered rectangular grid system indicated in **Fig. 2**, the following finite difference formulations are obtained for x and y sweep.
For x-sweep of Eqs. (27) and (28):

$$\frac{\lambda_1}{\Delta t/2}(S_{j,k}^{n+1/2}-S_{j,k}^{n})+\frac{\lambda_2}{2}\{(2-\delta)S_{j,k}^{n+1/2}+\delta S_{j,k}^{n}\}$$

$$+\frac{1}{2\Delta x}\{(2-\delta)(P_{j,k}^{n+1}-P_{j-1,k}^{n+1})+\delta(P_{j,k}^{n}-P_{j-1,k}^{n})\}$$

$$+\frac{1}{2\Delta y}\{(2-\delta_2)(Q_{j,k}^{n+1/2}-Q_{j,k-1}^{n+1/2})+\delta_2(Q_{j,k}^{n-1/2}-Q_{j,k-1}^{n-1/2})\}$$

$$+\frac{2i\omega}{CC_g}\left[U_{j,k}\frac{1}{2}\{(2-\delta)P_{j,k}^{n+1}+\delta P_{j,k}^{n}\}+V_{j,k}\frac{1}{2}\{(2-\delta_2)Q_{j,k}^{n+1/2}+\delta_2 Q_{j,k}^{n-1/2}\}\right]$$

$$=SS_{j,k}^{n+1/2} \tag{31}$$

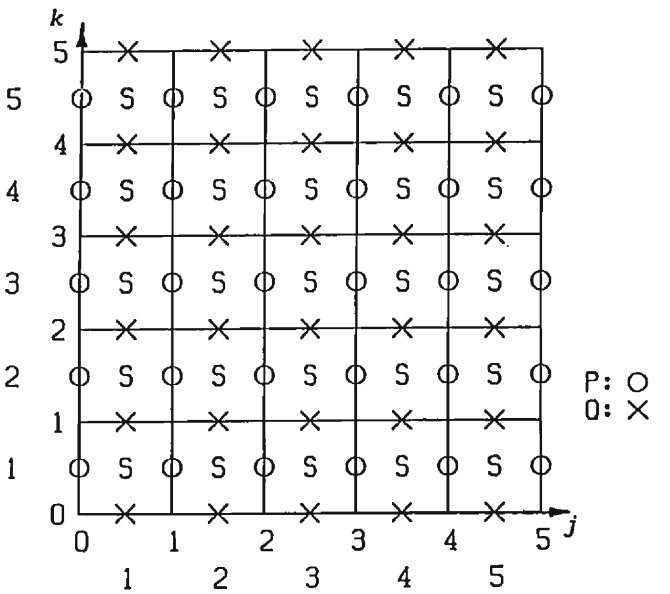

Fig. 2. Space-staggered grid system.
(○: pseudo flux $P_{j,k}$, ×: pseudo flux $Q_{j,k}$ and S: surface elevation $S_{j,k}$ and water depth)

$$\frac{\lambda_3}{\Delta t}(P_{j,k}^{n+1}-P_{j,k}^{n})+\frac{\lambda_4}{2}\{(2-\delta)P_{j,k}^{n+1}+\delta P_{j,k}^{n}\}$$

$$+C_g^2\frac{1}{\Delta x}(S_{j+1,k}^{n+1/2}-S_{j,k}^{n+1/2})=0 \tag{32}$$

where coefficients, λ_1, λ_2, λ_3, λ_4 are

$$\lambda_1=\frac{C_g}{C}+\frac{\omega^2-\sigma^2}{\omega^2}+i\left(\frac{U_{j,k}-U_{j-1,k}}{\Delta x}+\frac{V_{j,k}-V_{j,k-1}}{\Delta y}\right)+i\frac{W}{\omega}$$

$$\lambda_2=-i\omega\lambda_1,\qquad \lambda_3=\frac{C_g}{C},\qquad \lambda_4=-i\omega\frac{C_g}{C}$$

For y-sweep of Eqs. (27) and (29):

$$\frac{\lambda_1}{\Delta t/2}(S_{j,k}^{n+1}-S_{j,k}^{n+1/2})+\frac{\lambda_2}{2}\{(2-\delta)S_{j,k}^{n+1}+\delta S_{j,k}^{n+1/2}\}$$

$$+\frac{1}{2\Delta x}\{(2-\delta_2)(P_{j,k}^{n+1}-P_{j-1,k}^{n+1})+\delta_2(P_{j,k}^{n}-P_{j-1,k}^{n})\}$$

$$+\frac{1}{2\Delta y}\{(2-\delta)(Q_{j,k}^{n+3/2}-Q_{j,k-1}^{n+3/2})+\delta_2(Q_{j,k}^{n+1/2}-Q_{j,k-1}^{n+1/2})\}$$

$$+\frac{2i\omega}{CC_g}\left[U_{j,k}\frac{1}{2}\{(2-\delta_2)P_{j,k}^{n+1}+\delta_2 P_{j,k}^{n}\}+V_{j,k}\frac{1}{2}\{(2-\delta)Q_{j,k}^{n+1/2}+\delta Q_{j,k}^{n-1/2}\}\right]$$

$$=SS_{j,k}^{n+1} \tag{33}$$

$$\frac{\lambda_3}{\Delta t}(Q_{j,k}^{n+3/2}-Q_{j,k}^{n+1/2})+\frac{\lambda_4}{2}\{(2-\delta)Q_{j,k}^{n+3/2}+\delta Q_{j,k}^{n+1/2}\}$$

$$+C_g^2\frac{1}{\Delta y}(S_{j,k+1}^{n+1}-S_{j,k}^{n+1})=0 \tag{34}$$

where δ, δ_2 are weighting factors which indicate a complete implicit with $\delta=0$, the Crank-Nicolson with $\delta=1$ and an explicit scheme with $\delta=2$. Accurate solution are obtained by $\delta=1$ after certain number of iterations.

3.2 Double sweep algorithm

Eq. (31) can be rearranged with respect to unknown variables of $S_{j,k}^{n+1/2}$, $P_{j,k}^{n+1}$, $P_{j-1,k}^{n+1}$, as follows.

$$A_{1j,k}S_{j,k}^{n+1/2}+B_{j,K1}P_{j,k}^{n+1}+C_{j,k1}P_{j-1,k}^{n+1}=E_{1j,k} \tag{35}$$

where

$$A_{1j,k}=\lambda_1\frac{2}{\Delta t}+\frac{\lambda_2}{2}(2-\delta) \tag{36}$$

$$B_{1j,k}=\frac{2-\delta}{2\Delta x} \tag{37}$$

$$C_{1j,k}=-\frac{2-\delta}{2\Delta x} \tag{38}$$

$$\begin{aligned}E_{1j,k}=&\left(\lambda_1\frac{2}{\Delta t}-\frac{\lambda}{2}\,\delta\right)S^n_{j,k}-\frac{2}{2\Delta x}\delta(P^n_{j,k}-P^n_{j-1,k})\\&-\frac{2i\omega}{CC_g}\left[-\frac{1}{2\delta}\,\{(2-\delta_2)(Q^{n+1/2}_{j,k}-Q^{n+1/2}_{j,k-1})+\delta_2(Q^{n-1/2}_{j,k}-Q^{n-1/2}_{j,k-1})\}\right.\\&\left.+U_{j,k}\frac{1}{2}\,\{(2-\delta)P^{n+1}_{j,k}+\delta P^n_{j,k}\}+V_{j,k}\frac{1}{2}\,\{(2-\delta_2)Q^{n+1/2}_{j,k}+\delta_2 Q^{n-1/2}_{j,k}\}\right]\\&+SS^{n+1/2}_{j,k}\end{aligned} \tag{39}$$

On the other hand, Eq. (32) is rewritten as:

$$A_{2j,k}S^{n+1/2}_{j+1,k}+B_{2j,k}P^{n+1}_{j,k}+D_{2j,k}S^{n+1/2}_{j,k}=E_{2j,k} \tag{40}$$

where

$$A_{2j,k}=C_g^2\frac{1}{\Delta x} \tag{41}$$

$$B_{2j,k}=\frac{\lambda_3}{\Delta t}+\frac{\lambda_4}{2}\,(2-\delta) \tag{42}$$

$$C_{2j,k}=-C_g^2\frac{1}{\Delta x} \tag{43}$$

$$E_{2j,k}=\left(\frac{\lambda_3}{\Delta t}-\frac{\lambda_4}{2}\right)P^n_{j,k} \tag{44}$$

Eliminating S with Eqs. (35) and (40), we get a tridiagonal matrix with respect to P, as:

$$F_{1j,k}P^{n+1}_{j+1,k}+G_{1j,k}P^{n+1}_{j,k}+H_{1j,k}P^{n+1}_{j-1,k}=O_{1j,k} \tag{45}$$

where

$$F_{1j,k}=\frac{A_{2j,k}}{A_{1j,k}}\,B_{1j,k} \tag{46}$$

$$G_{1j,k}=\frac{A_{2j,k}}{A_{1j+1,k}}\,C_{1j,k}-B_{2j,k}+\frac{D_{2j,k}}{A_{1j,k}}\,B_{1j,k} \tag{47}$$

$$H_{1j,k}=\frac{D_{2j,k}}{A_{1j,k}}\,C_{1j,k} \tag{48}$$

$$O_{1j,k}=-E_{2j,k}+\frac{A_{2j,k}}{A_{1j+1,k}}E_{1j+1,k}+\frac{D_{2j,k}}{A_{1j,k}}E_{1j,k} \tag{49}$$

Eq. (45) can be quickly solved by the Thomas algorithm (the double sweep method). When $P_{j,k}^{n+1}$ is obtained, $S_{j,k}^{n+1/2}$ is directly calculated with Eq. (35).
In the case of y-sweep, Eqs. (33) and (34) can be solved by the same manner with respect to $Q_{j,k}^{n+3/2}$ and $S_{j,k}^{n+1}$.

3.3 Boundary conditions

For the actual calculation of wave fields in the coastal zone, three types of boundary condition have to be specified, such as wave generation, absorption and reflection. The developed model in this study can introduce these conditions as follows.

(a) Wave generation boundary

As mentioned in the previous section, wave generation can be incorporated into the model system in terms of the source term SS of the equivalent mass conservation equation, which is defined as:

$$SS=\frac{\Delta_S}{\Delta x\Delta y}CS_0 \tag{50}$$

where S_0 is the complex surface elevation function along a generation line, which is defined as

$$S_0=A_0e^{i\chi_0} \tag{51}$$

where χ_0 is phase function described as:

$$\chi_0=\vec{k}\cdot\vec{x} \tag{52}$$

Using this boundary condition, it is possible to generate waves with arbitrary height, wave number and direction.

(b) Wave absorption boundary (sponge layer)

For engineering applications the computational domain has to be limited as small as possible. One possibility to achieve this demand is introducing an artificial absorption boundary. The so-called sponge layer developed by Larsen and Dancy (1983)[10] in their short wave paropagation model is employed here to absorb all outgoing waves at an open boundary. After each time (iteration) step, the surface elevation and pseudo fluxes are divided with artificial function $\mu(x)$. The function used in this paper is

$$\mu(x)=\begin{cases}\exp\{(2^{-x/\Delta x}-2^{-x_s/\Delta x})\ln\alpha\} & \text{for} \quad 0\leqq x\leqq x_s\\ 1 & \text{for} \quad x_s\leqq x\end{cases} \tag{53}$$

where x_s is the sponge layer width and α is a constant that depends on the number of grids inside the sponge layer described by $x_s/\Delta x$.

(c) Wave reflection boundary

The perfect reflection is achieved by

$$Q=0 \quad \text{or} \quad P=0 \tag{54}$$

However, an arbitrary reflection boundary condition is often needed in the calculation of short waves around coastal structures. It is possible to get an analytical reflection coefficient for one-dimensional difference equation system as shown by Madsen and Larsen (1987)[8], but this problem is not treated here.

4. Fundamental tests of the model

In order to confirm the basic characteristics of the developed model, (1) wave height in the surf zone (breaking test), (2) effective application technique of the sponge layer (sponge layer test) and (3) external/internal diffraction tests are examined.

4.1 Wave breaking test

Wave height variation in the surf zone is the most important information for near-shore dynamics. The wave propagation model elaborated in section 2 includes the effect of energy dissipation due to breaking. Computed breaker height variation in the surf zone is examined by comparing with previous experiments. For this purpose the one-dimensional numerical wave flume with uniformly sloping bottom (1/30) is set up as shown in **Fig. 3** in which wave generator (generation term) is located at the left end of the flume. The sponge layers ($\alpha=10$, $x_s/\Delta x=5$) are located at the back of numerical wave generator and at the end of slope.

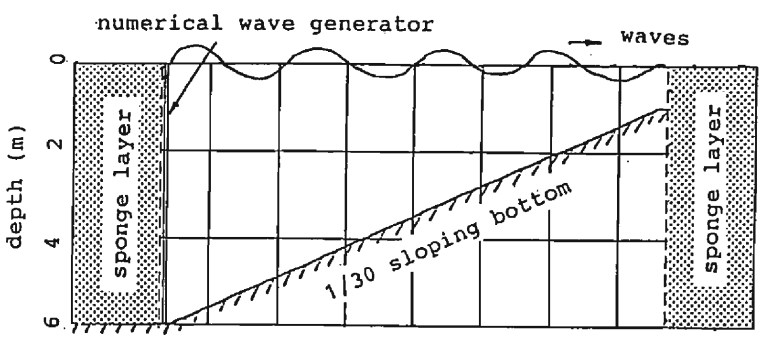

Fig. 3. Numerical wave flume for one-dimensional wave breaking tests.

Since the energy dissipation term suddenly affects at the breaking point, a numerically reflected waves (disturbances) are generated at this point. Thick broken line in **Fig. 4** indicates an example of the unrealistic disturbances, where significantly reflected waves (left-going waves) are observed.

To eliminate this numerical reflection, a smoothing funcition is operated to the

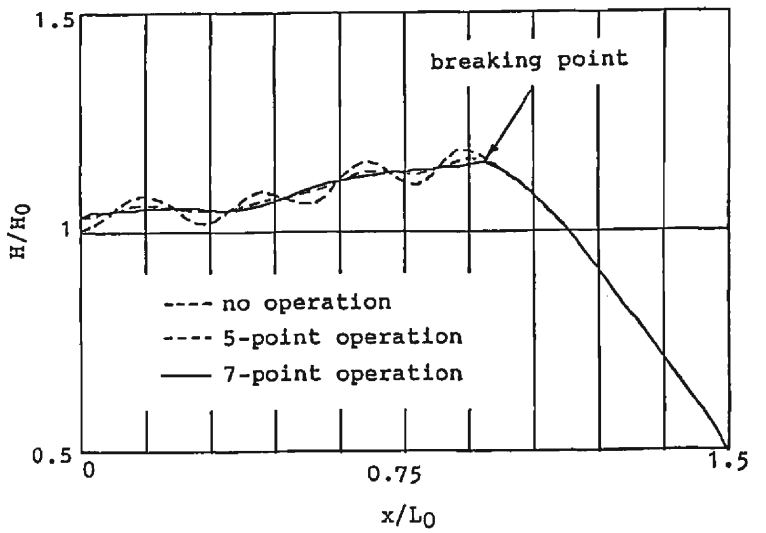

Fig. 4. Elimination of numerical reflection due to wave energy dissipation term W.

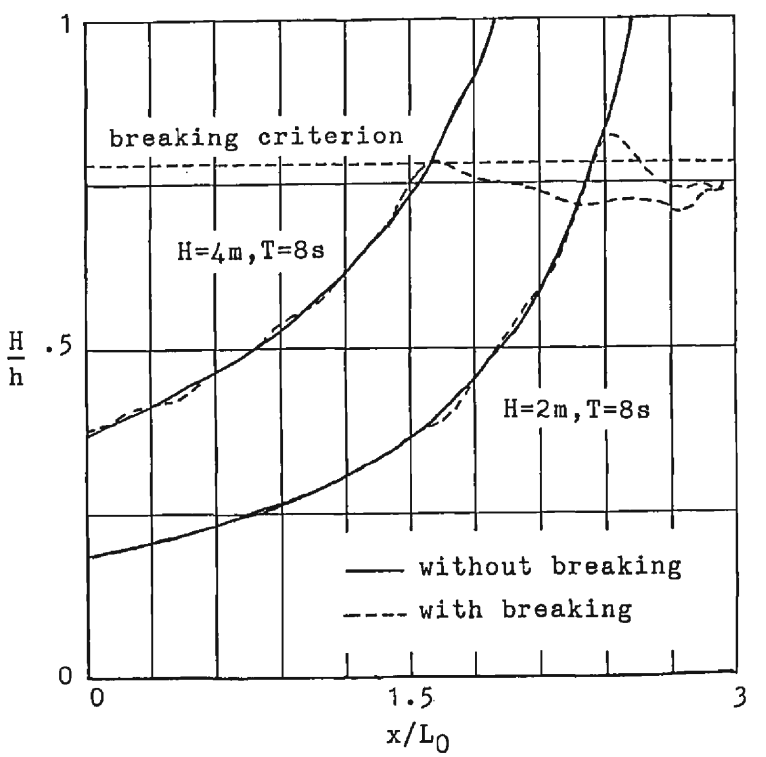

Fig. 5. Breaking points estimated by the time-dependent MSE model and the method used in this study.

dissipation term W. Assuming the linear smoothing function, 5- and 7-point operation centering the breaking point are examined. The resultant wave height variatioin is in **Fig. 4.** It is recognized that 7-point operation of the smoothing function works well in eliminating numerical reflection and it does not affect the wave height decay inside the surf zone.

As employed in the time-dependent MSE model by Watanabe et al. (1984)[14], the breaking point is specified after caluculating the whole region without consideration of wave breaking. By this method the wave height in the surf zone has to be calculated twice. To avoid this loss of computing time breaking and reforming judgement is performed by the ratio of local wave height to depth in the preceding iteration step. Difference in results by the former and latter methods is examined and shown in **Fig. 5** for two cases, $H_0=2$ m, $T=8$ s, and $H_0=4$ m, $T=8$ s. The breaking criterion of $H_B/h_B=0.78$ is used. No significant difference in wave height variations is observed in both cases and it can be concluded that the latter method is applicable to determine the breaking point.

Test of breakier height variation is carried out to confirm the applicability of breaking term used in the model. **Fig. 6** shows the comparison of wave height variation between calculations and experiments. **Fig. 6(a)** is the result of typical spilling breaker ($H_0/L_0=0.04$, bottom slope$=1/30$) and the case of spiller/plunger transition ($H_0/L_0=0.02$, bottom slope$=1/30$). It is observed that the calculations explain experimental data within an allowable range except wave heights near the breaking point, where difference between the linear theory and experiments inherently exists because of wave profile peaking near the crest.

4.2 Sponge layer test

The radiation condition is usually employed at the open boundary to scatter all outgoing waves. The technique of sponge layer based on an artificial damping is employed here, which enable an economical calculation for engineering applications to reduce the computational domain.

Larsen and Dancy (1983)[10] employed this technique in a computation of short wave field by means of dividing S and P (or Q) with the disspation function $\mu(x)$ after each iteration step. Madesen and Larsen (1987)[8] used a liner friction factor in the sponge layer of their H-MSE numerical model.

Equal wave height lines in the constant depth are shown in **Figs. 7(a)** and **(b)**, which depict effectiveness and drawback of the sponge layer, respectively. Almost perfect absorption is achieved within several grids of sponge layer for normal wave incidence (**Fig. 7(a)**) and no disturbance is observed in it. In the case of side-wall boundary, however, wave diffraction due to sponge layer causes undesirable disturbance in the calculation domain, as shown in **Fig. 7(b)**. Therefore, attention has to be made in setting the sponge layer not to generate such an undesirable disturbance. Sometimes selection of the boundary conditions is not so easy in the practical problems.

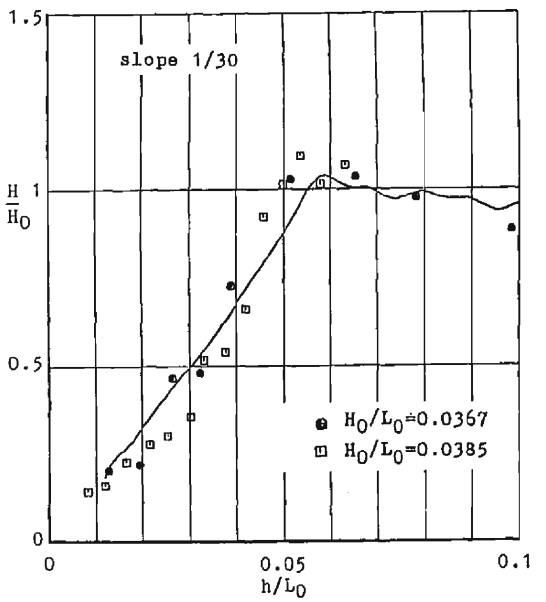

(a) $H_0/L_0=0.04$ (calculation)

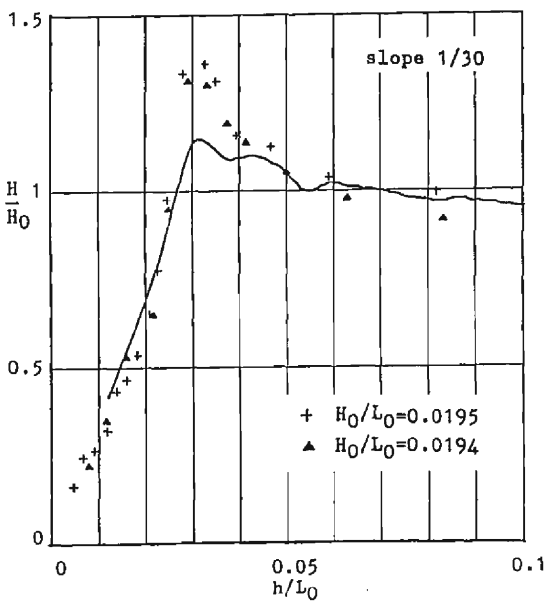

(b) $H_0/L_0=0.02$ (calculation)

Fig. 6. Comparison of breaking wave heights between caluculations and experiments.

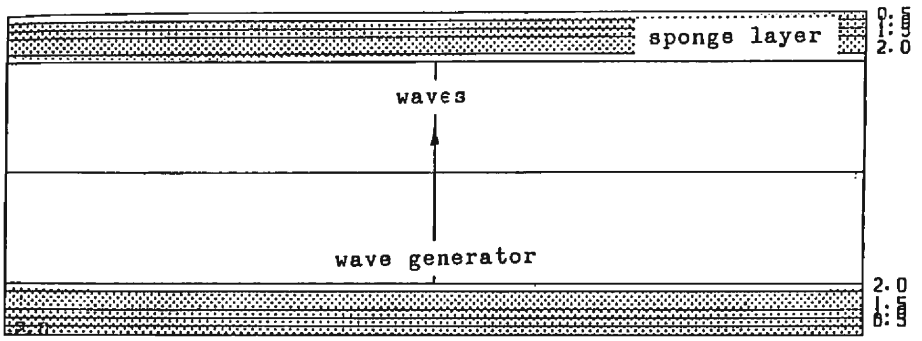

(a) Normal incidence and the fixed side boundaries.

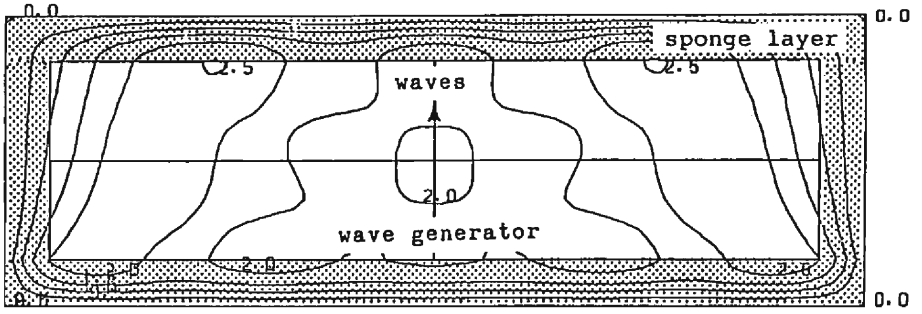

(b) Normal incidence and the sponge layer side boundaries.

Fig. 7. Effectiveness and drawback of the sponge layer.

4.3 Internal diffraction test

The most common test to examine the diffraction (internal diffraction) and refraction combined problem is the elliptical shoal test. **Fig. 8** is the test setup used by the Delft Hydraulics Laboratory (1982)[15] in which the elliptical shoal described by Eq. (55) is located on the uniformly sloping bottom.

$$h(x, y)=h_1(x, y)+h_2(x, y) \tag{55}$$

where

$$h_1(x, y)=\frac{7}{360}(\sin 20°x+\cos 20°y)$$

$$h_2(x, y)=0.3-\frac{1}{2}\sqrt{1-\left(\frac{x-10.75}{5}\right)^2-\left(\frac{y-15}{3.75}\right)^2}$$

in the region: $\left(\frac{x-10.75}{5}\right)^2+\left(\frac{y-15}{3}\right)^2\leqq 1$

$h_2(x, y)=0$ otherwise

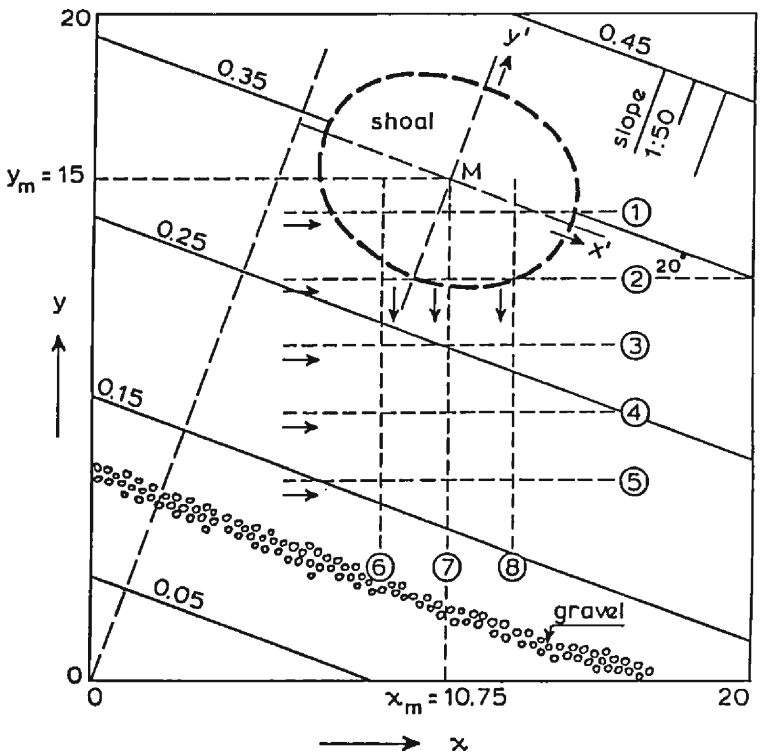

Fig. 8. Setup of the elliptical shoal experiments[15] and sections along which wave heights are compared with calculations.

The comparison between calculations and experiments conducted by the Delft Hydraulics Laboratory[15] is made. **Fig. 9** shows the results of experiment. The result of the developed model is shown in **Fig. 10.** Wave height distributions along the specified lines are shown in **Fig. 11** comparing with the Delft Hydraulics Laboratory's experimental data. From these figures, it can be observed that the calculated wave height after passing the elliptical shoal are higher than the experimental results, however their convergence-divergence tendency is pretty good comparing with previous studies. It may be concluded that the numerical model has a well applicability to the problem combined the internal diffraction and refraction.

4.4 External diffraction test

Reflection-diffraction (external diffraction) combined wave field is formed around emerged coastal structures. The test of external diffraction is conducted to examine the model's applicability to this problem, assuming the perfect reflection from the strucuture, constant water depth and normal incidence. **Fig. 12** shows the reflection-diffraction wave field calculated by Born et al. (1965)[16] **Fig. 12(a)** and by the model developed in this study **Fig. 12(b)**. The former is the numerical evaluation of the Som-

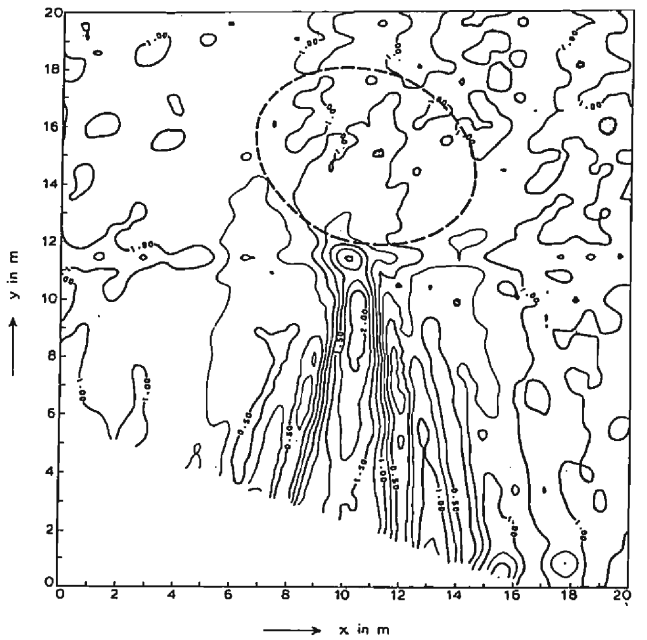

(a) Wave height distribution

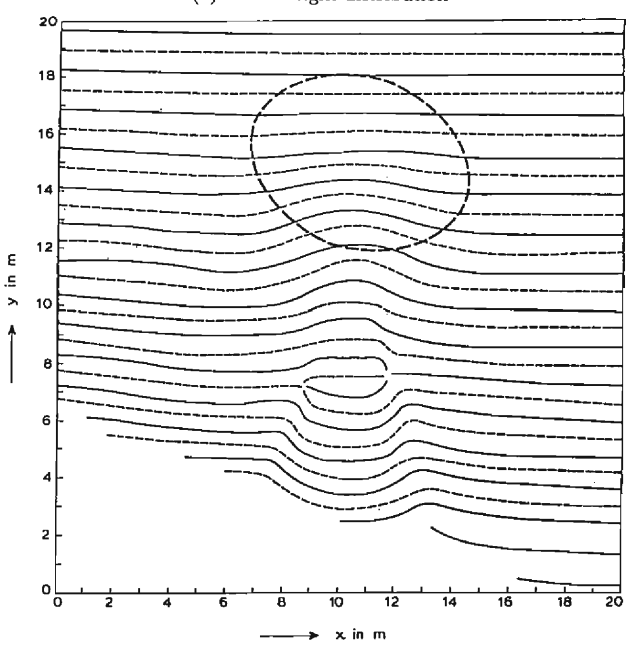

(b) Equal phase lines

Fig. 9. Results of the elliptical shoal experiment[15].

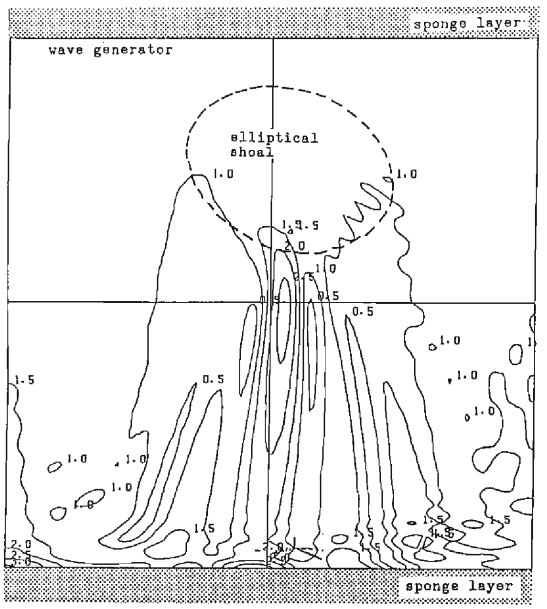

(a) Wave height distribution

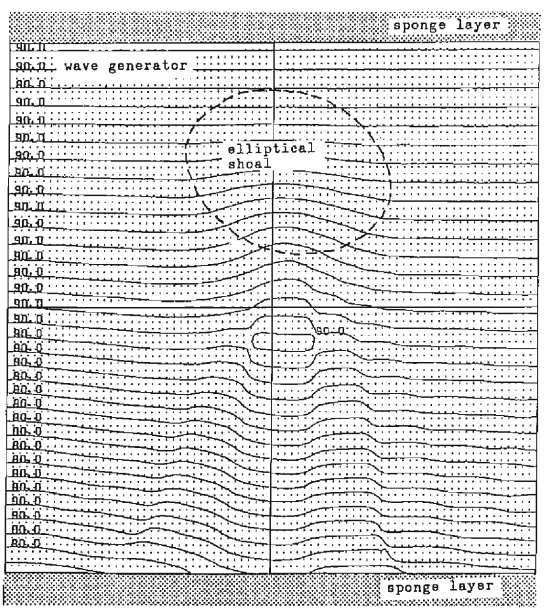

(b) Equal phase lines

Fig. 10. Numerical results of the elliptical shoal test.

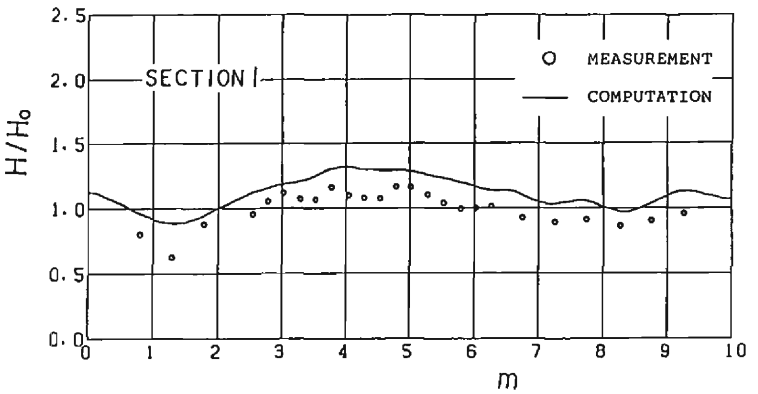

(a) Section 1

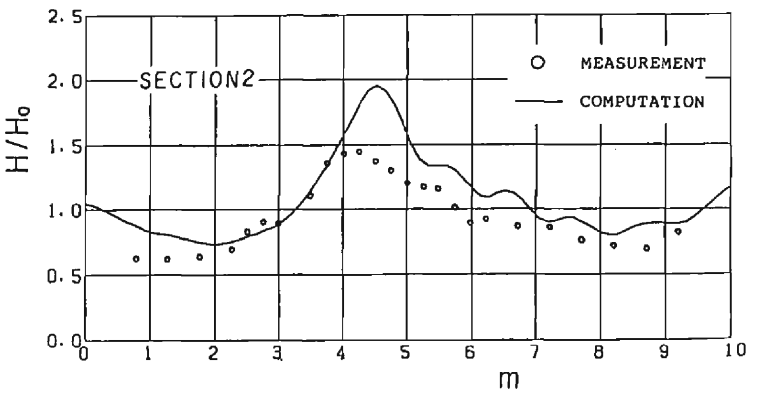

(b) Section 2

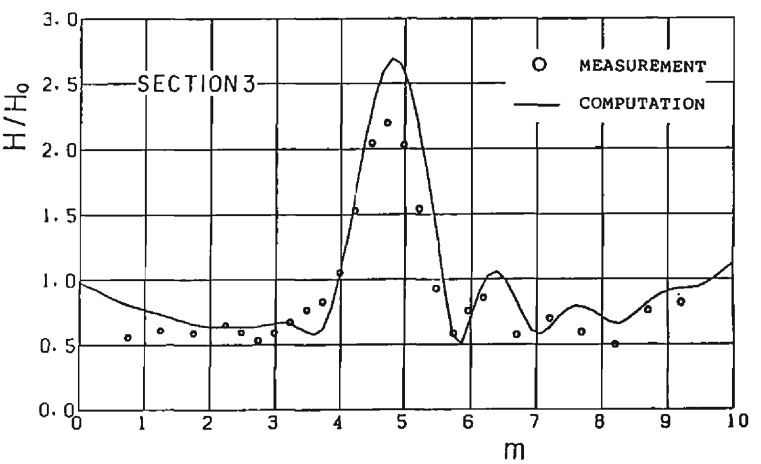

(c) Section 3

Fig. 11. continued

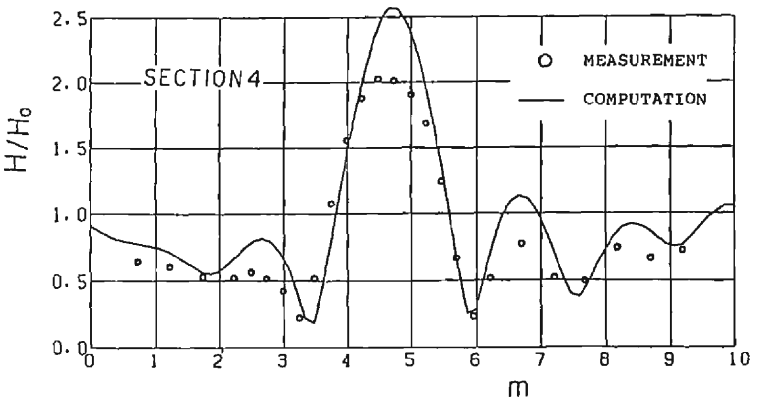

(d) Section 4

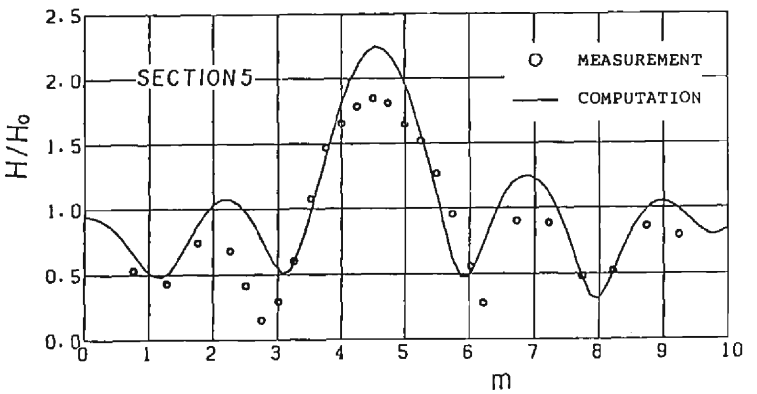

(e) Section 5

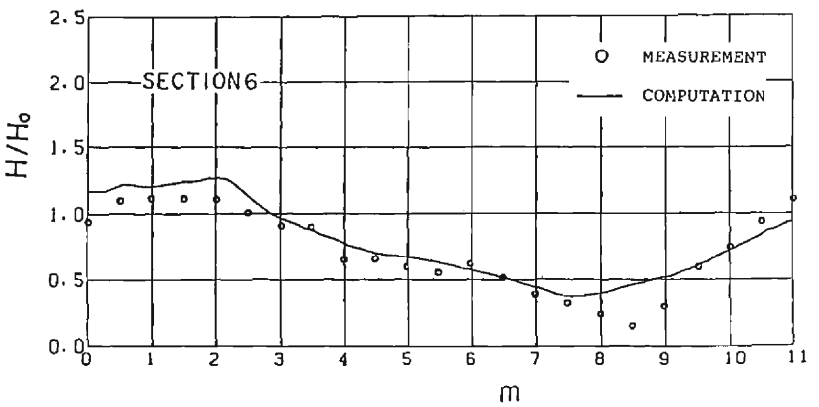

(f) Section 6

Fig. 11. continued

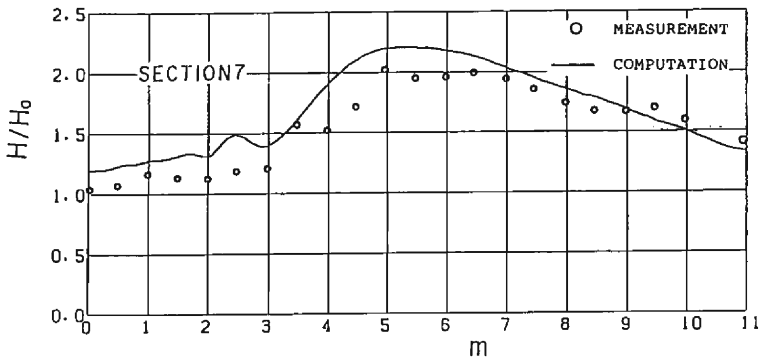

(g) Section 7

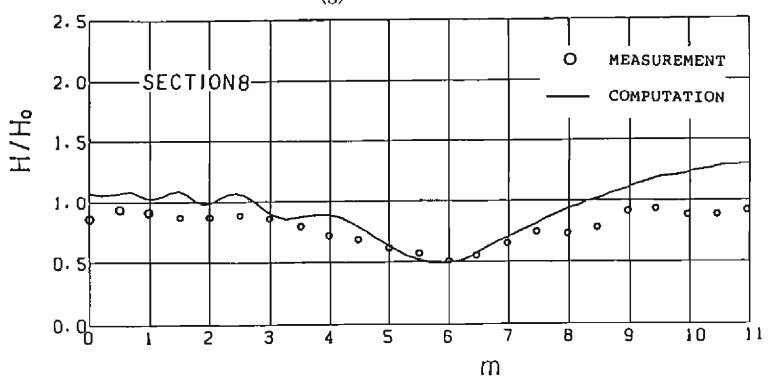

(h) Section 8

Fig. 11. Comparison of wave height distributions between calculations and experiments by the Delft Hydraulics Laboratory[15].

merfeld solution and the latter is the numerical solution of the model developed where the sponge layer boundary condition is used. The figure shows that the sponge layer somewhat affects the wave field near the end boundary. However, the wave field in the domain of interest may be simulated with allowable accuracy.

4.5 Example of application

An application of the model is demonstrated in **Fig. 13** assuming the condition that normal wave incidence of wave period 16 s, height lm, into shallow water where a strucuture combined offshore breakwater and fishery harbour exists. **Fig. 13(a)** shows wave height distribution and **Fig. 13(b)** the equal phase lines (wave direction).

As the perfect reflecton from the strucutre is assumed in this calculation, wave height just in front of offshore breakwater seems to be extrememly large. However, judging from the figure, no significant disturbances by the sponge layer can be observed.

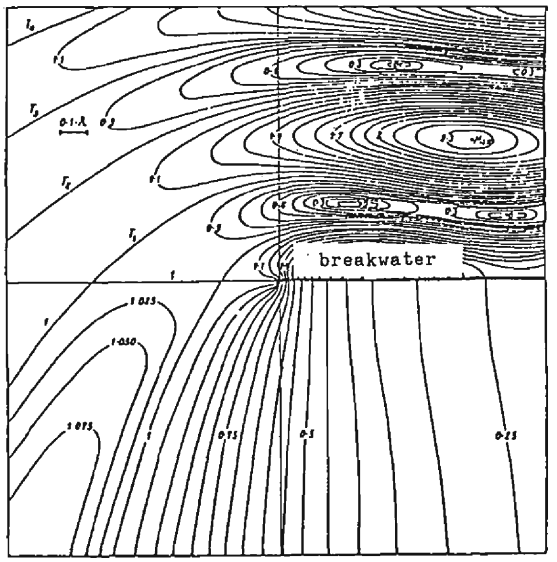

(a) Theoretical results by Born et al.[16]

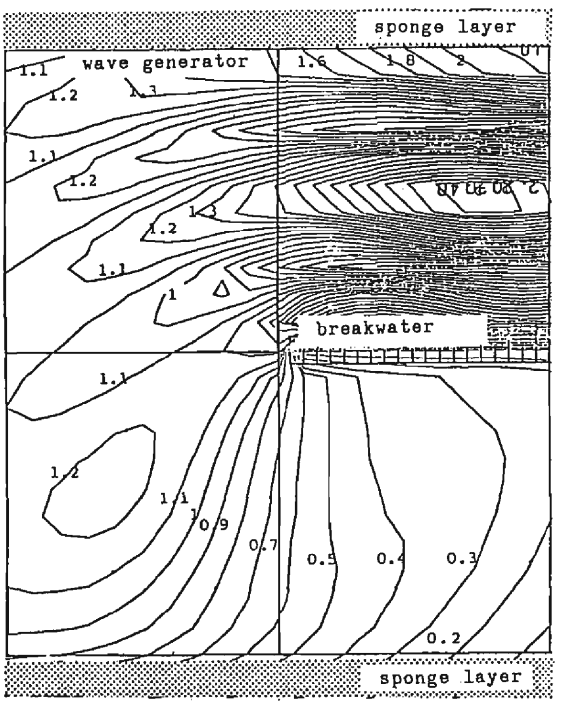

(b) Numerical results by this study

Fig. 12. Diffraction by a semi-finite breakwater.

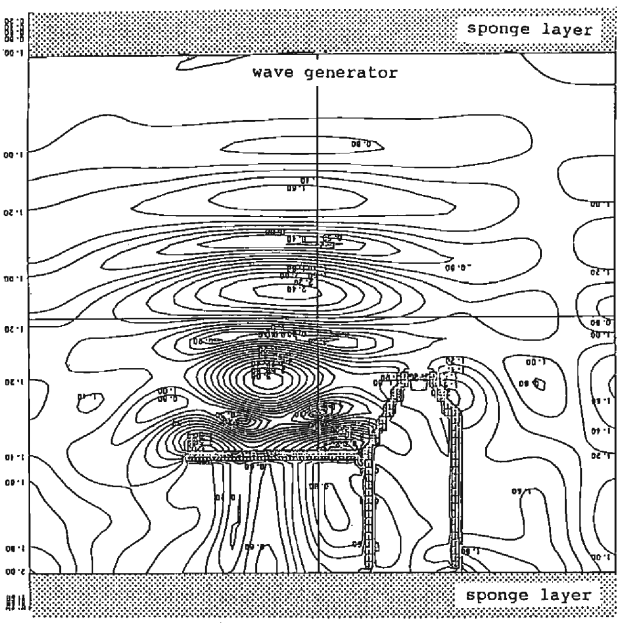

(a) Wave height distribution

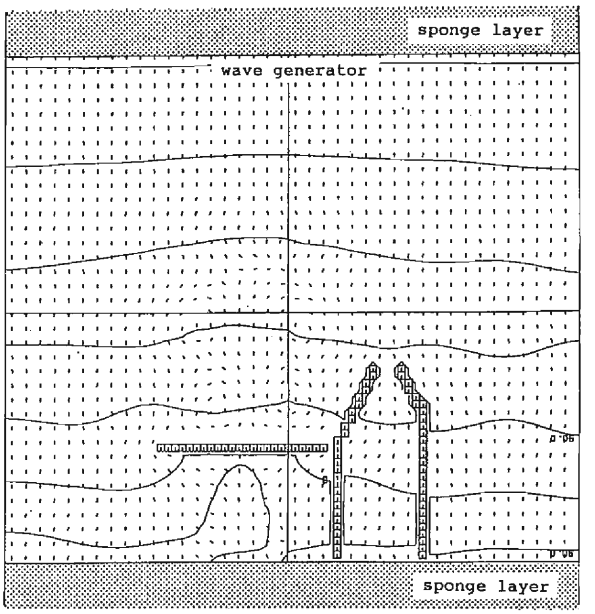

(b) Equal phase line

Fig. 13. Wave fields in the areas around coastal structures (offshore breakwater and fishery harbour).

5. Conclusions

Numerical calculation method of short waves in the coastal zone was developed using the transformed mild equation (H-MSE), which was derived by transforming the elliptic MSE into the system of three first-order hyperbolic equations. Including additional effects of energy dissipation due to wave breaking and wave-current interaction, the version-up of the model was achieved to simulated the wave field in the surf zone as well as around the coastal structures with an accuracy for engineering practices. A highly efficient ADI algorithm was used iteratively to get the stationary solution in which effects of refraction, diffraction, reflection and energy disspation are simultaneously considered.

Acknowledgement

The work described in this paper was supported by the Grant-in-Aid for Scientific Research from the Ministry of Education, Science and Culture of Japan, under Grant No. 62302045.

References

1) Abbott, M. B., Petersen, H. M. and Skovgaad, O.: On the numerical modelling of short waves in shallow water, Jour. Hydraulic Res., Vol. 16, No. 3, 1978, pp. 173–204.
2) Berkhoff, J. C. W.: Computations of combined refraction-diffraction, Proc. 13th Int. Conf. on Coastal Eng., Chap. 24, 1972, pp. 471–490.
3) Berkhoff, J. C. W.: Mathematical models for simple harmonic linear water waves, Delft Hydraulics Laboratory, Publ. No. 163., 1976, p. 103.
4) Radder, A. C.: On the parabolic equation method for water-wave propagation, Jour. Fluid Mech., Vol. 95, No. 1, 1979, pp. 159–176.
5) Tsuchiya, Y., T. Yamshita and A. Yamamoto: Numerical calculation method of parabolic-approximated mild slope equation and its applications, Proc. of 34th Japanese Conf. on Coastal Eng., JSCE, 1987, pp. 96–100 (in Japanese).
6) Warren I. R., Larsen J. and Madesen, P. A.: Application of short wave numerical models to harbour design and future development of the model, Int. Conf. on Numerical and Hydraulic Modelling of Ports and Harbours, Birmingham, 1985.
7) Copeland, G. J. M.: A practical alternative to the mild-slope wave equations, Coastal Engineering, Vol. 9, 1985, pp. 125–149.
8) Madesen, P. A. and Larsen, J.: An efficient finite difference approach to the mild slope equation, Coastal Engineering, Vol. 11, 1987, pp. 329–351.
9) Ito, Y. and Tanimoto, K.: A method of numerical analysis of wave propagation—application to wave diffraction and refraction, Proc. 13th Int Conf. on Coastal Eng., ASCE, Chap. 26, 1972, pp. 503–522.
10) Larsen J. and Dancy, H.: Open boundaries in short-wave simulation. A new approach, Coastal Engineering, Vol. 7, 1983, pp. 285–297.
11) Kirby, J. T. and Dalrymple, R. A.: An approximate model for nonlinear dispersion in monochromatic wave propagation model, Coastal Engineering, Vol. 9, 1986, pp. 545–561.
12) Kirby, J. T.: A note on linear surface wave current interaction slowly varying topography, Jour. Geophy. Res., Vol. 89, C1, 1984, pp. 745–747.
13) Izumiya, T. and Horikawa, K.: Wave energy equation applicable in and outside the surf zone, Coastal Eng. in Japan, Vol. 27, 1984, pp. 119–137.

14) Watanabe, A. and Y. Maruyama: Numerical calculation method of refraction-diffraction combined equation with energy dissipation due to breaking, Proc. of 31st Japanese Conf. on Coastal Eng., JSCE, 1984, pp. 103–107 (in Japanese).
15) Delft Hydraulics Laboratory: Refraction and diffraction of water waves; wave deformation by a shoal; comparison between computations and measurements, Report W154, part VIII, 1982, p. 19.
16) Born, M. and E. Wolf: Principles of optics, Pergamon Press, 1965, pp. 556–592.